J. Math. Computer Sci., 37 (2025), 132–153

Online: ISSN 2008-949X

Journal of Mathematics and Computer Science

Journal Homepage: www.isr-publications.com/jmcs

A comparative study of numerical methods for singularly perturbed boundary value problems

Kamran[a,*], Salma Aljawi[b], Muhammad Irfan[a], Dania Santina[c,*], Nabil Mlaiki[c,*]

[a]Department of Mathematics, Islamia College Peshawar, Peshawar 25120, Khyber Pakhtoonkhwa, Pakistan.

[b]Department of Mathematical Sciences, Princess Nourah Bint Abdulrahman University, P.O. Box 84428, Riyadh 11671, Saudi Arabia.

[c]Department of Mathematics and Sciences, Prince Sultan University, P.O. Box 66833, Riyadh 11586, Saudi Arabia.

Abstract

Singularly perturbed boundary value problems (SPBVPs) plays an important role in modeling various phenomena in engineering and other science fields. The aim of this article is to compare the performance of numerical methods applied to solve the SPBVPs, which are challenging due to the presence of small perturbation parameters leading to boundary or interior layers. Four numerical methods are compared, namely, the local radial basis function method, the improved Talbot's method, the Euler's method, and the Weeks method. The main objective of this work is to improve the stability and accuracy of solutions for SPBVPs, which are important for many applications in science and engineering. We consider two-point SPBVPs with a boundary layer at one endpoint. To evaluate the performance and effectiveness of the presented numerical techniques, numerical approximations of four SPBVPs are derived and compared with the analytical solutions. The results presented in the tables and figures validate that the proposed numerical schemes are highly accurate and clearly outperform the outcomes of other methods. Furthermore, results from the functional analysis were used to study the existence of the solution to the considered model and generate sufficient requirements for Ulam-Hyers stability.

Keywords: Singularly perturbed BVPs, local radial basis functions, Laplace transform, Euler's method, improved Talbot's method, Weeks method.

2020 MSC: 34Bxx, 34Cxx, 34D15, 44A10.

1. Introduction

Singularly perturbed differential equations (SPBVPs) plays vital role in various scientific fields [32]. SPBVPs are those problems that have one or more delay term or in which the highest order derivative is multiplied by a small parameter [26]. The small parameter significantly effect the behavior of the solution. SPBVPS are challenging because as the small parameter approaches zero, the solutions can vary rapidly, which often leads to boundary layers where the solution changes sharply. Problems of this type arise when the past and present, as well as the future, are interdependent. Such equations have applications in modeling of different phenomena like, the study of bistable devices [29], physiological processes [22], computational neuroscience [39], control theory [4, 16], blood cell production [28], etc.

*Corresponding author

Email addresses: kamran.maths@icp.edu.pk (Kamran), dsantina@psu.edu.sa (Dania Santina), nmlaiki@psu.edu.sa, nmlaiki2012@gmail.com (Nabil Mlaiki)

doi: 10.22436/jmcs.037.02.01

Received: 2024-05-28 *Revised:* 2024-06-19 *Accepted:* 2024-07-08

Many researchers have examined the numerical solution of SPBVPs, such as, Debela et al. [10] developed an accurate numerical method for SPBVPs. Ahsan et al. [5] developed a higher-order Haar wavelet method for approximating the solution of nonlinear SPBVPs with various types of boundary conditions. For the first time Pearson [36] solved the SPBVPs including turning points problems numerically by taking net adjustment via finite difference method. The author of [14] investigated a brand-new replicating kernel-based approach to a class of singularly SPBVPs. Ramos et al. [40] utilized an unconventional approach to numerically solve nonlinear SPBVPs on nonuniform models. Vigo-Aguiar and Natesans [56] obtained the solution for solitary perturbation problems via exponentially fitted difference scheme. The authors in [37] tackled a non-iterative numerical integration solution for SPBVPs representing an internal and twin boundary layer. The solution of stiff SPBVPs with twin boundary layers was discussed in [23]. Jayakumar et al. [31] presented a uniform numerical approach for SPBVPs with boundary layers. Hammachukiattikul et al. [18] obtained the approximate solution of singularly perturbed advanced-delay convection-diffusion type differential equations via the finite and hybrid difference schemes. The existence and asymptotic stability of periodic solutions with an interior layer of reaction-advection-diffusion equations have been examined by Nefedov et al. [33]. Debela and Duressa [11] developed a finite difference method for studying the numerical solution of SPBVPs with non-local boundary conditions. More information on the investigation of SPBVPs are reported in [9, 30, 38, 55] and references therein.

In this article, we study the numerical solution to the SPBVPs using the localized radial basis function method (LRBFM) and the Laplace transform methods (LTM) [2, 47, 61]. The LRBFM is the most practical and effective method for variety of single and multi variate boundary value problems. LRBFM has gained attention of the research community over other approaches due to its quick convergence, simplicity of implementation, low computational cost, ease of understanding, and versatility to higher dimensions [42]. Different real world problems have been solved using the LRBFM, such as the authors of [50] used the LRBFM to approximate the solution of hyperbolic PDEs. Noorizadegan et al. [35] utilized the LRBFM for solving the piezoelectric medium problems. In [60] the authors used LRBFM for spatial-temporal calcium dynamics. Wei et al. [58] studied the solution of variable order fractional diffusion equations via LRBFM. In [41] used the LRBFM with optimal shape parameter for fractional order integro differential equations. Nikan et al.[34] developed a stable LRBFM for diffusion equations of time fractional order arising in mass and heat transfer. More information on the application of LRBFM are reported in [6, 8, 24]. Key features of the LRBFM are following.

- LRBFM divides the domain into sub-domains and constructs interpolants within each sub-domain.
- LRBFM does not require structured mesh, it uses scattered nodes.
- LRBFM can effectively capture steep gradients and boundary layers.
- LRBFM results in a system of linear equation that can be solved numerically.
- LRBFM can handle multi-dimensional complex problems.

The disadvantages of LRBFM are: (i) this method can be computationally expensive; (ii) if the basis functions are not selected carefully, this technique may result in an ill-conditioned system. The other technique used in this article is the Laplace transform technique for the purpose to compare the results using LRBFM with the results of Laplace transform.

Laplace transform (LT) has been proved to be the finest mathematical tool used for solving linear ODEs and PDEs in engineering and other sciences. LT has applications in the field of physics, control engineering, electrical engineering, and signal processing [49]. However, while using the LT, the main problem is obtaining its inverse. The inverse of LT is not well posed and its analytic inversion for complicated functions is not available. Thus, a numerical technique must be utilized for its inversion. Many numerical techniques are developed that can be used for the inversion of LT, such as the Fourier series technique[20], the Zakian's technique [17], the Weeks technique [59], the Stehfest's technique [51], the

Talbot's method technique [52], etc. The Laplace inversion methods have been utilized by many authors for various problems (see [19, 25, 45, 46]). However, the Talbot's and Stehfest's methods are among the popular methods frequently used for the inversion of LT for many problems arising in engineering and other sciences. Some key features of LT method are given as follows.

- LT method is analytic that transforms the problem from time domain to frequency domain.
- Solves the transformed problem in frequency domain.
- Using the LT inversion technique get back the time domain solution.
- LT method can effectively solve initial value problems.
- For many problems LT can provide closed-form solutions, it can also handle impulsive forces and discontinuities via the Dirac delta and Heaviside functions.

The disadvantages of LT method are: (i) LT cannot handle nonlinear problems; (ii) LT may face problems in solving problems with variable coefficients or complex boundary conditions; (iii) for complex function the inversion can be challenging. In this article, we study the application of the LRBFM, the Talbot's method [12], the Euler's method [1], and the Weeks method [59] for a second order SPBVP of the form ([7])

$$\epsilon\delta_1\frac{d^2u(\tau)}{d\tau^2}+\delta_2\frac{du(\tau)}{d\tau}+\delta_3u(\tau)=f(\tau),\ \tau\in\Omega, \tag{1.1}$$

or it can be expressed more simply as

$$\mathcal{L}u(\tau)=f(\tau), \tag{1.2}$$

where $\mathcal{L}=\epsilon\delta_1\frac{d^2}{d\tau^2}+\delta_2\frac{d}{d\tau}+\delta_3$ with Dirichlet's boundary conditions

$$\mathcal{B}u(\tau)=g_1(\tau),\ \tau\in\partial\Omega, \tag{1.3}$$

and initial condition

$$u(0)=\phi_1,\ u'(0)=\phi_2, \tag{1.4}$$

where $\delta_1,\delta_2,\delta_3$ are the coefficients, $f(\tau)$ $g_1(\tau)$, $u(0)$ are given sufficiently continuous differentiable functions. Furthermore, we assume that $\delta_2\geqslant q_1$ throughout the domain Ω, where $q_1>0$ which implies the boundary layer will be at left of the domain, and if $\delta_2\leqslant q_1<0$ the boundary layer will be at the right end of the domain. Solution of SPBVPs have a multi-scale character, i.e., there are thin transition layers where the solution changes fast is known inner region, and the where the solution changes slowly is known outer region.

2. Existence of solution

In this section, we examine the existence and uniqueness of the solution to the problem (1.1)-(1.4).

Lemma 2.1 ([57]). *Let $f\in C(\mathcal{T},R)$, where $\mathcal{T}=[0,T]$, then the function $u(\tau)$ is a solution of the integral equation*

$$u(\tau)=\phi_1+\tau\phi_2+\int_0^\tau(\tau-s)\left[\lambda_1f(s)-\lambda_2\frac{du(s)}{ds}-\lambda_3u(s)\right]ds,\ \tau\in\mathcal{T},$$

if and only if $u(\tau)$ is the solution of problem (1.1)-(1.4), where $\lambda_1=\frac{1}{\epsilon\delta_1}$, $\lambda_2=\frac{\delta_2}{\epsilon\delta_1}$, $\lambda_3=\frac{\delta_3}{\epsilon\delta_1}$.

Proof. To achieve our goal we first set the problem defined in (1.1)-(1.4) as

$$u''(\tau)=h(\tau), \tag{2.1}$$

where $h(\tau) = \left[\lambda_1 f(s) - \lambda_2 \frac{du(s)}{ds} - \lambda_3 u(s)\right]$ is a is a continuous function. Integrating both sides of (2.1) from 0 to τ yields

$$u'(\tau) - u'(0) = \int_0^\tau h(s)ds,$$

or equivalently

$$u'(\tau) = \phi_2 + \int_0^\tau h(s)ds. \tag{2.2}$$

Integration of (2.2) from 0 to τ yields

$$u(\tau) - u(0) = \phi_2\tau + \int_0^\tau \int_0^\tau h(s)dsds,$$

or equivalently

$$u(\tau) = \phi_1 + \phi_2\tau + \int_0^\tau (\tau - s)h(s)ds,$$

or equivalently

$$u(\tau) = \phi_1 + \phi_2\tau + \int_0^\tau (\tau - s)\left[\lambda_1 f(s) - \lambda_2 \frac{du(s)}{ds} - \lambda_3 u(s)\right]ds.$$

□

To introduce the Ulam-Hyers stability, we consider the following inequality:

$$\left|\frac{d^2\bar{u}(\tau)}{d\tau^2} - F\left(\frac{d\bar{u}(\tau)}{d\tau}, \bar{u}(\tau), f(\tau)\right)\right| < \varepsilon. \tag{2.3}$$

Definition 2.2 ([54]). A solution of problem (1.1)-(1.4) admits Ulam-Hyers stability if there exist a positive real number μ_k such that for every solution $\bar{u}$ of the inequality (2.3), there exist an exact solution u such that $\|u - \bar{u}\| < \mu_k\varepsilon$.

To transform the problem to a fixed point, we define the operator $\mathcal{S} : \Omega \to \Omega$ such that

$$\mathcal{S}u(\tau) = \phi_1 + \tau\phi_2 + \int_0^\tau (\tau - s)\left[\lambda_1 f(s) - \lambda_2 \frac{du(s)}{ds} - \lambda_3 u(s)\right]ds,$$

the solutions of the problem (1.1) are the fixed points of the operator $\mathcal{S}$. For further analysis we need the following assumptions. For any $\tau \in [0, T]$ there exist constants m_1, m_2, m_3, m_4 such that

(A1) $|\frac{du_1}{d\tau} - \frac{du_2}{d\tau}| \leqslant m_1|u_1 - u_2|$;
(A2) $|\frac{du}{d\tau}| \leqslant m_2|u|$;
(A3) $|f(\tau, u_1, u_2) - f(\tau, \bar{u}_1, \bar{u}_2)| \leqslant m_3|u_1 - \bar{u}_1| + m_4|u_2 - \bar{u}_2|$.

Theorem 2.3 (Schauder's fixed point theorem, [3]). *Let $\mathfrak{T}$ be a nonempty, convex, compact subset of a Banach space Ω and let $\mathcal{S} : \mathfrak{T} \to \mathfrak{T}$ is a compact operator that maps $\mathfrak{T}$ into itself. Then, $\mathcal{S}$ has a fixed point in $\mathfrak{T}$.*

The integral form of (1.1) is given as

$$u(\tau) = \phi_1 + \tau\phi_2 + \int_0^\tau (\tau - s)\left[\lambda_1 f(s) - \lambda_2 \frac{du(s)}{ds} - \lambda_3 u(s)\right]ds, \ \tau \in \mathcal{T}.$$

Since f is bounded linear function so $|f(\tau)| \leqslant \mathcal{C}_f$, $\mathcal{C}_f > 0$.

Theorem 2.4. *Using the hypothesis* (A1)-(A2), *the problem* (1.1) *has a solution.*

Proof. To prove the desired result we define the Banach space Ω equipped with norm define by $\|u\| = \sup_{\tau\in\mathcal{T}}|u(\tau)|$. Let us define $\mathfrak{T}$ as $\mathfrak{T} = \{u \in \Omega : \|u\| \leqslant \sigma\}$, where $\sigma \geqslant \frac{2(|\phi_1|+|\phi_2|T^2)+T^3|\lambda_1|\mathcal{C}_f}{2-T^2(|\lambda_2 m_2|+|\lambda_3|)}$ and the operator $\mathcal{S} : \mathfrak{T} \to \mathfrak{T}$ by

$$\mathcal{S}[u(\tau)] = \phi_1 + \phi_2\tau + \int_0^\tau (\tau - s)[\lambda_1 f(s) - \lambda_2\frac{du(s)}{ds} - \lambda_3 u(s)]ds, \ \tau \in \mathcal{T}. \tag{2.4}$$

We need to show that $\mathfrak{T}$ is bounded, let $u \in \mathfrak{T}$, then we have using Eq. (2.4),

$$\begin{aligned}
|u(\tau)| &= \left|\phi_1 + \phi_2\tau + \int_0^\tau (\tau - s)\left[\lambda_1 f(s) - \lambda_2\frac{du(s)}{ds} - \lambda_3 u(s)\right]ds\right| \\
&\leqslant |\phi_1| + |\phi_2||\tau| + \int_0^\tau (\tau - s)\left[|\lambda_1||f(s)|ds + |\lambda_2||m_2||u(s)| + |\lambda_3||u(s)|\right]ds \\
&\leqslant |\phi_1| + |\phi_2|T^2 + \frac{T^2|\lambda_1|\mathcal{C}_f}{2} + \frac{T^2(|\lambda_2 m_2| + |\lambda_3|)}{2}\|u\| \leqslant \sigma,
\end{aligned}$$

thus $\|u\| \leqslant \sigma$. This demonstrates the boundedness of $\mathcal{S}$. It is obvious that $\mathcal{S}$ maps bounded set into bounded sets. Next, we prove that $\mathcal{S}$ is continuous, suppose u_n in $\mathfrak{T}$, since $\mathfrak{T}$ is a closed and compact set. So, $u_n \to u$, as $n \to \infty$. Therefore, we have

$$\begin{aligned}
|\mathcal{S}u_n(\tau) - \mathcal{S}u(\tau)| &= \int_0^\tau (\tau - s)\left[\lambda_1 f(s) - \lambda_2\frac{du_n(s)}{ds} - \lambda_3 u_n(s)\right]ds \\
&\quad - \left(\int_0^\tau (\tau - s)\left[\lambda_1 f(s) - \lambda_2\frac{du(s)}{ds} - \lambda_3 u(s)\right]ds\right) \\
&\leqslant \int_0^\tau (\tau - s)|\lambda_2|\left|\frac{du_n(s)}{ds} - \frac{du(s)}{ds}\right| + |\lambda_3||u_n(s) - u(s)|ds \\
&\leqslant \int_0^\tau (\tau - s)\Big(|\lambda_2|m_1 + |\lambda_3|\Big)|u_n(s) - u(s)|ds \\
&\leqslant \frac{\tau^2}{2}\Big(|\lambda_2|m_1 + |\lambda_3|\Big)\|u_n(s) - u(s)\|_\infty.
\end{aligned}$$

Since u is continuous, we have $\|\mathcal{S}u_n - \mathcal{S}u\| \to 0$, as $n \to 0$. Hence $\mathcal{S}$ is continuous. Next, let $\tau_1, \tau_2 \in \mathcal{T}$, then we have

$$\begin{aligned}
&|\mathcal{S}u(\tau_2) - \mathcal{S}u(\tau_1)| \\
&= \left|\int_0^{\tau_2} (\tau_2 - s)\left[\lambda_1 f(s) - \lambda_2\frac{du(s)}{ds} - \lambda_3 u(s)\right]ds - \left(\int_0^{\tau_1} (\tau_1 - s)\left[\lambda_1 f(s) - \lambda_2\frac{du(s)}{ds} - \lambda_3 u(s)\right]ds\right)\right| \\
&\leqslant \int_0^{\tau_1} [(\tau_2 - s) - (\tau_1 - s)]|\lambda_1 f(s) - \lambda_2\frac{du(s)}{ds} - \lambda_3 u(s)|ds + \int_{\tau_1}^{\tau_2} [(\tau_2 - s)]|\lambda_1 f(s) - \lambda_2\frac{du(s)}{ds} - \lambda_3 u(s)|ds.
\end{aligned}$$

Thus

$$\begin{aligned}
|\mathcal{S}u(\tau_2) - \mathcal{S}u(\tau_1)| &\leqslant \left(\frac{\tau_2^2}{2} - \frac{\tau_1^2}{2} + \frac{(\tau_2 - \tau_1)^2}{2} - \frac{(\tau_2 - \tau_1)^2}{2}\right)(\lambda_1\mathcal{C}_f + \lambda_2 m_2\sigma + \lambda_3\sigma) \\
&= \frac{(\lambda_1\mathcal{C}_f + \lambda_2 m_2\sigma + \lambda_3\sigma)}{2}(\tau_2^2 - \tau_1^2).
\end{aligned}$$

We see that if $\tau_2 \to \tau_1$, then $\tau_2^2 - \tau_1^2 \to 0$, then right hand side of the above equation also tends to zero. Therefore, $|\mathcal{S}u(\tau_2) - \mathcal{S}u(\tau_1)| \to 0$ as $\tau_2 \to \tau_1$. Since $\mathcal{S}$ continuous and bounded so it is uniformly continuous. Hence, $\|\mathcal{S}u(\tau_2) - \mathcal{S}u(\tau_1)\| \to 0$ as $\tau_2 \to \tau_1$. Hence $\mathcal{S}$ is equi-continuous, and therefore, by

Arzelà-Ascoli Theorem $\mathcal{S}$ is relatively compact. Therefore, the operator $\mathcal{S}$ has atleast one fixed point by Schauder's fixed point theorem. Thus, problem (1.1) has a solution. □

3. Stability

We develop the stability results for problem (1.1) in this part. The concept of UH stability is crucial for real-world issues in biology, economics, and physics. Consider the problem

$$u(\tau) = \phi_1 + \tau\phi_2 + \int_0^\tau (\tau - s)\left[\lambda_1 f(s) - \lambda_2 \frac{du(s)}{ds} - \lambda_2 u(s) + g(s)\right] ds, \ \tau \in \mathcal{T}, \tag{3.1}$$

where $g \in \Omega$ and $|g(\upsilon)| \leqslant \epsilon$ for $\epsilon > 0$, then (3.1) has a solution

$$u(\tau) = \phi_1 + \tau\phi_2 + \int_0^\tau (\tau - s)\left[\lambda_1 f(s) - \lambda_2 \frac{du(s)}{ds} - \lambda_2 u(s) + g(s)\right] ds. \tag{3.2}$$

Using Theorem 2.4, (3.2) can be written as

$$u(\tau) = \mathcal{S}u(\tau) + \int_0^\tau (\tau - s) g(s) ds, \tau \in \mathcal{T}.$$

From equation (3.2), using (3.1), one has $|\mathcal{S}u(\tau) - u(\tau)| \leqslant \epsilon\frac{\tau^2}{2}$.

Theorem 3.1. *Problem* (1.1)-(1.4) *is UH and generalized UH stable if* $\frac{\tau^2\epsilon}{2-\tau^2(|\lambda_2|m_1+|\lambda_3|)} < 1$.

Proof. Let $u, \bar{u} \in \Omega$ be exact and approximate solutions of (1.1)-(1.4), respectively, then

$$\begin{aligned}\|u - \bar{u}\| = \sup_{\tau\in\mathcal{T}} |u(\tau) - \mathcal{S}\bar{u}(\tau)| &\leqslant \sup_{\tau\in\mathcal{T}} |u(\tau) - \mathcal{S}u(\tau)| + \sup_{\tau\in\mathcal{T}} |\mathcal{S}u(\tau) - \mathcal{S}\bar{u}(\tau)| \\ &\leqslant \frac{\tau^2}{2}\epsilon + \frac{\tau^2}{2}\Big(|\lambda_2|m_1 + |\lambda_3|\Big)\|u - \bar{u}\| \leqslant \frac{\tau^2\epsilon}{2 - \tau^2(|\lambda_2|m_1 + |\lambda_3|)}.\end{aligned}$$

□

4. Numerical scheme

We consider two different approaches: (i) the LRBFM; (ii) the LT methods.

4.1. The local radial basis function method (LRBFM)

In LRBFM the problems domain and its boundary are interpolated on N_r points. For each point $\tau_i (i = 1, 2, 3, \ldots, N_r)$, there is a local domain $\Omega_i = \{\tau_j^i\}_{j=1}^{ns} (j = 1, 2, 3, \ldots, ns, ns < N_r)$, where n is the total number of points in the local domain Ω_i. Hence, the approximation of $u(\tau)$ using LRBFM has the form

$$u(\tau_i) = \sum_{j=1}^{ns} \beta_j^i \psi(\|\tau_i - \tau_j^i\|),$$

where $\boldsymbol{\beta}^i = \{\beta_j^i\}_{j=1}^{ns}$ represents the unknown coefficients, $\psi(r)$ is kernel function, and $r = \|\tau_i - \tau_j^i\|$, $\Omega_i \subset \Omega$. Many kernel functions are proposed in literature. Some of them are presented in Table 1, and their graphs for different values of the shape parameter are presented in Figures 1-4.

Table 1: Different types of RBFs.

Linear spline	$\psi(r,\upsilon) = \upsilon r$
Cubic spline	$\psi(r,\upsilon) = (\upsilon r)^3$
Quadric (Q-RBF)	$\psi(r,\upsilon) = 1+\upsilon^2 r^2$
Multiquadric (MQ-RBF)	$\psi(r,\upsilon) = \sqrt{1+\upsilon^2 r^2}$
Inverse multiquadric (IMQ-RBF)	$\psi(r,\upsilon) = \frac{1}{\sqrt{1+\upsilon^2 r^2}}$
Gaussian(GA-RBF)	$\psi(r,\upsilon) = e^{-(\upsilon r)^2}$

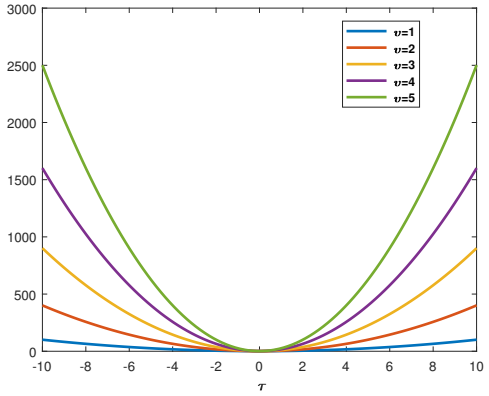

Figure 1: The plots Q-RBF in the domain $[-10,10]$ with different values of the shape parameter υ.

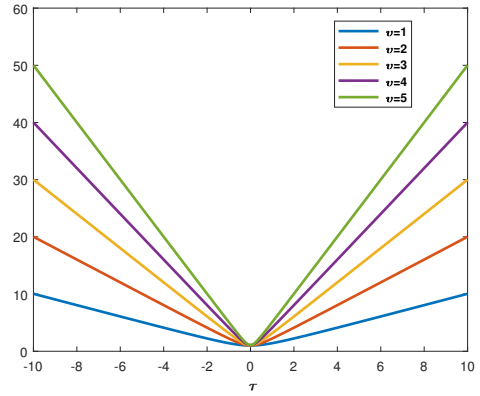

Figure 2: The plots MQ-RBF in the domain $[-10,10]$ with different values of the shape parameter υ.

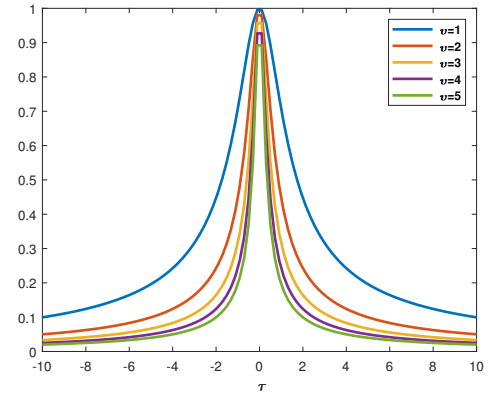

Figure 3: The plots IMQ-RBF in the domain $[-10,10]$ with different values of the shape parameter υ.

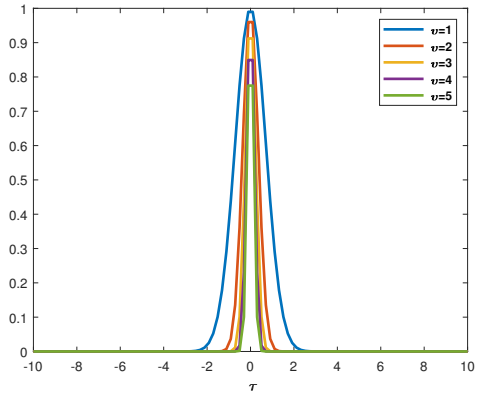

Figure 4: The plots GA-RBF in the domain $[-10,10]$ with different values of the shape parameter υ.

In this study, the MQ-RBF defined as $\psi(r,\upsilon) = \sqrt{1+\upsilon^2 r^2}$ are selected, the sub-domain Ω_i has the center τ_j^i and its $n-1$ neighboring centers around it. A one dimensional five points stencil is shown in Figure 5.

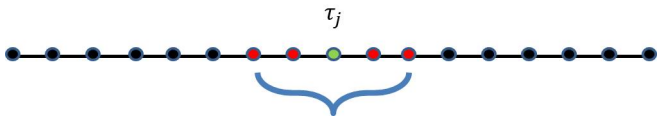

Figure 5: A five points stencil.

Hence, we have $n \times n$ systems given as

$$\begin{pmatrix} u(\tau_1^i) \\ u(\tau_2^i) \\ . \\ . \\ . \\ u(\tau_{ns}^i) \end{pmatrix} = \begin{pmatrix} \psi_{11} & \psi_{12} & . & . & . & \psi_{1ns} \\ \psi_{21} & \psi_{22} & . & . & . & \psi_{2ns} \\ . & . & . & . & . & . \\ . & . & . & . & . & . \\ . & . & . & . & . & . \\ \psi_{ns1} & \psi_{ns2} & . & . & . & \psi_{nsns} \end{pmatrix} \begin{pmatrix} \beta_1^i \\ \beta_2^i \\ . \\ . \\ . \\ \beta_{ns}^i \end{pmatrix}, \ i = 1, 2, \ldots, N_r,$$

which can be written as

$$\mathbf{u}^i = \mathbf{\Psi}^i \boldsymbol{\beta}^i, \tag{4.1}$$

where $\mathbf{\Psi}^i$ has elements of the form $b_{kj}^i = \psi(\|\tau_k^i - \tau_j^i\|)$, where $\tau_k^i, \tau_j^i \in \Omega_i$. It has been reported in literature that the system matrix $\mathbf{\Psi}^i$ is non singular, if the points in the stencil are all distinct and $\upsilon \neq 0$ ([27]). Thus the coefficients $\boldsymbol{\beta}^i$ in (4.1) can be computed as

$$\boldsymbol{\beta}^i = (\mathbf{\Psi}^i)^{-1} \mathbf{u}^i \tag{4.2}$$

Also for $\mathcal{L}$ we have

$$\mathcal{L}u(\tau_i) = \sum_{\tau_j \in \Omega_i} \beta_j^i \mathcal{L}\psi(\|\tau_i - \tau_j^i\|). \tag{4.3}$$

From Eq. (4.3), we have

$$\mathcal{L}u(\tau_i) = \boldsymbol{\nu}^i \cdot \boldsymbol{\beta}^i, \tag{4.4}$$

where $\boldsymbol{\beta}^i$ and $\boldsymbol{\nu}^i$ are vectors of order $ns \times 1$ and $1 \times ns$, where the elements $\boldsymbol{\nu}^i$ are of the form

$$\boldsymbol{\nu}^i = \mathcal{L}\psi(\|\tau_i - \tau_j^i\|), \ \tau_j^i \ \in \Omega_i.$$

From (4.2) and (4.4), we have

$$\mathcal{L}u(\tau_i) = \boldsymbol{\nu}^i (\Psi^i)^{-1} \mathbf{u}^i = \mathbf{\Phi}^i \mathbf{u}^i,$$

where

$$\mathbf{\Phi}^i = \boldsymbol{\nu}^i (\mathbf{\Psi}^i)^{-1}. \tag{4.5}$$

Hence, the linear differential operator $\mathcal{L}$ is approximated via LRBFM at each point τ_i as

$$\mathcal{L}u \equiv \mathbf{D}_{\mathcal{L}} \mathbf{u}, \tag{4.6}$$

where $\mathbf{D}_{\mathcal{L}}$ is a sparse differentiation matrix. We can obtain the approximation of $\mathcal{L}_{\mathcal{B}}$ in a similar way as

$$\mathcal{B}u \equiv \mathbf{D}_{\mathcal{B}} \mathbf{u}, \tag{4.7}$$

using (4.6) and (4.7) in (1.2) and (1.3) we have the following system

$$\mathbf{D}_{\mathcal{L}} \mathbf{u} = f(\tau), \quad \mathbf{D}_{\mathcal{B}} \mathbf{u} = g_1(\tau). \tag{4.8}$$

Solving the system defined in (4.8) we will obtain the desired numerical solution.

4.1.1. Selecting best shape parameter

There are numerous radial kernel functions that can be found in the literature. In this article, we have used the multiquadric radial basis function (MQ-RBF) which is defined as $\psi(r, \upsilon) = \sqrt{1 + \upsilon^2 r^2}$. The MQ-RBF includes υ known as the shape parameter. The approximate solutions' accuracy is linked with the value of this parameter. Many algorithms are proposed in literature for obtaining the best value of υ. In this article we have used the uncertainty principle due to [43] for selecting the best value of υ. The key

steps are explained in Table 2,

Table 2: Algorithm for selecting best shape parameter.

Input	$\mathcal{K}_{\min}$, $\mathcal{K}_{\max}$, $d\upsilon$
Step i	$\mathcal{K} = 1$
Step ii	choose $10^{+12} < \mathcal{K} < 10^{+16}$
Step iii	while $\mathcal{K} > \mathcal{K}_{\max}$ and $\mathcal{K} < \mathcal{K}_{\min}$
Step iv	construct the interpolation matrix $\mathbf{\Psi}^p$
Step v	$\mathbf{U}, \mathbf{S}, \mathbf{V} = \text{svd}(\mathbf{B}^p)$
Step vi	$\mathbf{C} = \frac{\rho_{\max}}{\rho_{\min}}$
Step vii	if $\mathcal{K} < \mathcal{K}_{\min}, \upsilon = \upsilon - d\upsilon$
Step viii	if $\mathcal{K} > \mathcal{K}_{\max}, \upsilon = \upsilon + d\upsilon$
Output	$\upsilon(\text{best}) = \upsilon$

where $\mathcal{K}$ is the condition number of the system matrix $\mathbf{\Psi}^i$, υ is the shape parameter, and $d\upsilon$ is the increment in υ. The inverse $(\mathbf{\Psi}^i)^{-1}$ is computed using svd as $(\mathbf{\Psi}^i)^{-1} = (\mathbf{USV^T})^{-1} = \mathbf{VS^{-1}U^T}$ (see [53]). Hence we can calculate $\mathbf{\Phi}^i$ in (4.5).

4.2. The Laplace transform method

LT has been used by many researchers for studying the solution of differential equations arising in physics and engineering. The LT of $u(\tau)$ is defined as

$$\widehat{u}(s) = \mathscr{L}\{u(\tau)\} = \int_0^\infty e^{-s\tau} u(\tau) d\tau,$$

where s denotes the LT parameter, and the quantities in Laplace space are denoted by an over wide hat. The LT of n^{th} derivative of $u(\tau)$ be given as

$$\mathscr{L}\left\{\frac{d^n u(\tau)}{d\tau^n}\right\} = s^n \widehat{u}(s) - s^{n-1}u(0) - s^{n-2}u'(0) - \cdots - u^n(0).$$

Employing the LT to (1.1)-(1.3), we get

$$\begin{aligned}&\mathscr{L}\left\{\epsilon\delta_1 \frac{d^2u(\tau)}{d\tau^2} + \delta_2 \frac{du(\tau)}{d\tau} + \delta_3 u(\tau)\right\} = \mathscr{L}\{f(\tau)\}\\ &\Rightarrow \epsilon\delta_1[s^2\widehat{u}(s) - su(0) - u'(0)] + \delta_2[s\widehat{u}(s) - u(0)] + \delta_3\widehat{u}(s) = \widehat{f}(s),\end{aligned}$$

or

$$\left(\epsilon\delta_1 s^2 + \delta_2 s + \delta_3\right)\widehat{u}(s) = \epsilon s u(0) + \epsilon u'(0) + u(0) + \widehat{f}(s).$$

After simplifying the above we get

$$\widehat{u}(s) = \frac{\widehat{F}(s)}{\epsilon\delta_1 s^2 + \delta_2 s + \delta_3}, \tag{4.9}$$

where $\widehat{F}(s) = \epsilon s u(0) + \epsilon u'(0) + u(0) + \widehat{f}(s)$. After applying the inverse LT to Eq. (4.9) we get $u(\tau)$ as

$$u(\tau) = \frac{1}{2\pi i}\int_{\rho - i\infty}^{\rho + i\infty} e^{s\tau}\widehat{u}(s) ds = \frac{1}{2\pi i}\int_\Gamma e^{s\tau}\widehat{u}(s) ds, \tag{4.10}$$

where Γ is a contour extending from $\rho - i\infty$ to $\rho + i\infty$ for $\rho > 0$, falling to the right of all the singularities of $\widehat{u}(s)$ in the complex s-plane. The main concern is to compute the integral in (4.10), furthermore, we

use the numerical methods for its inversion. When an analytical inversion of Laplace domain solution is not available, a numerical inversion technique must be used. The Laplace inversion can be carried out via a variety of algorithms that are reported in the literature. Every technique is appropriate for a specific function and has its own merits. The integral given in Eq. (4.10) is evaluated using approximations in all inversion techniques. The three commonly used inversion algorithms are presented in the sections that follow.

4.2.1. The improved Talbot's method (ITM)

Talbot's approach for numerically inverting the LT involves integrating the Bromwich integral defined in (4.10) numerically via the trapezoidal or mid point rule along a special contour Γ. These rules when coupled with contour deformation can effectively evaluate the integral defined in Eq. (4.10). The contour is deformed for the purpose to handle the exponential factor in Eq. (4.10). Consider, for example, that the integration path in (4.10) can be deformed to a Hankel contour, where the real part of the contour starts at $-\infty$ in the 3rd quadrant, winds around all the singularities of $\widehat{u}(s)$, and ends with the real part again heading to $-\infty$ in the 2nd quadrant. The integral in Eq. (4.10) is especially well-suited for approximation by the trapezoidal or midpoint rules on such contours because the exponential factor induces a quick decrease. As long as the contour stays inside the range of analyticity of the $\widehat{u}(s)$, Cauchy's theorem can be used to justify such deformation. Additionally, some conditions on the decay of the transform function $\widehat{u}(s)$ in the left half-plane are necessary [52]. In literature various contours have been proposed such as parabola [13] and hyperbola [48]. In this work, we use the contour proposed in [12] having the parametric form given as

$$\Gamma : s = s(\rho), \qquad -\pi \leqslant \rho \leqslant \pi,$$

$Re(\pm\pi) = -\inf$, and $s(\rho)$ is given as

$$s(\rho) = \frac{N_t}{\tau}\zeta(\rho), \ \zeta(\rho) = -\delta + \sigma\rho\cot(\mu\rho) + \gamma i\rho, \tag{4.11}$$

where the parameters $\mu, \sigma, \delta, \gamma$ must be selected by the authors. Eqs. (4.11) and (4.10) give

$$u(\tau) = \frac{1}{2\pi i}\int_{-\pi}^{\pi} e^{s(\rho)\tau}\widehat{u}(s)(s(\rho))s'(\rho)d\rho. \tag{4.12}$$

We can now use the mid point rule with step $h = \frac{2\pi}{N_t}$ to approximate the integral in Eq. (4.12) as

$$u_{ApSol}(\tau) \approx \frac{1}{iN_t}\sum_{j=1}^{N_t} e^{s(\rho_j)\tau}\widehat{u}(s(\rho_j))s'(\rho_j), \qquad \rho_j = -\pi + (j - \frac{1}{2})h. \tag{4.13}$$

4.2.2. Error analysis

The following theorem provides details of the error analysis of improved Talbot's technique.

Theorem 4.1 ([12]). *Let ρ_j be defined as in (4.13). Let $f : \Theta \to \mathbb{C}$ be analytic in the set*

$$\Theta = \{\rho \in \mathbb{C} : -\pi < Re(\rho) < \pi \text{ and } -c_1 < Im(\rho) < c_2\},$$

when $c_2, c_1 > 0$, then

$$\int_{-\pi}^{\pi} f(\rho)d\rho - \frac{2\pi}{N_t}\sum_{j=1}^{N_t} f(\rho_j) = G_-(\alpha) + G_+(\beta),$$

here

$$G_+(\alpha) = \frac{1}{2}\left(\int_{-\pi}^{-\pi+i\alpha} + \int_{-\pi+i\alpha}^{\pi+i\alpha} + \int_{\pi+i\alpha}^{\pi}\right)\left(1 + i\tan\left(\frac{N_t\rho}{2}\right)\right) f(\rho)d\rho,$$

and

$$G_-(\beta) = \frac{1}{2}\left(\int_{-\pi}^{-\pi-i\beta} + \int_{-\pi-i\beta}^{\pi-i\beta} + \int_{\pi-i\beta}^{\pi}\right)\left(1 - i\tan\left(\frac{N_t\rho}{2}\right)\right) f(\rho)d\rho,$$

$\forall 0 < \alpha < c_2$, *and* $0 < \beta < d_1$ *and* N_t *even, if* N_t *is an odd number,* $\tan(\frac{N_t\rho}{2})$ *can be replaced with* $-\cot(\frac{N_t\rho}{2})$, *if* $f(\bar{\rho}) = \overline{f(\rho)}$, *and* c_2 *and* c_1 *can be taken to be equal, then*

$$G(\beta) = G_+(\beta) + G_-(\beta) = Re\int_{-\pi+i\beta}^{\pi+i\beta}\left(1 + i\tan\left(\frac{N_t\rho}{2}\right)\right) f(\rho)d\rho,$$

Through the analysis of the behavior of complex tangent function, we have

$$|G(\beta)| \leqslant \frac{4\pi\mathcal{M}}{\exp(c_2N_t) - 1},$$

the above results are obtained for even N_t, *for an odd* N_t *we can have similar results,* $\mathcal{M}, c_2 \in \mathbb{R}^+$.

For optimal solution, the most effective integration contour is necessary, which may be derived by deriving the best values of the parameters involved in (4.11). In [12] the following optimal values of the parameters were derived

$$\gamma = \frac{2645}{10000}, \quad \mu = \frac{6407}{10000}, \quad \delta = \frac{6122}{10000}, \quad \text{and} \quad \sigma = \frac{5017}{10000}.$$

The error estimate is given as

$$Err_{est} = |u(\tau) - u_{ApSol}(\tau)| = O(e^{-1.3580N_t}).$$

4.2.3. Euler's method (EM)

Euler's method (EM) is Fourier series method implementation that uses Euler summation for quick convergence. Since the Fourier series technique can be obtained from the integral in (4.10). In EM for a given Laplace transform $\widehat{u}(s)$ of a function $u(\tau)$ the approximation $u_{ApSol}(\tau)$ is expressed as

$$u_{ApSol}(\tau) = \frac{10^{\frac{N_e}{3}}}{\tau}\sum_{k=0}^{2N_e}\beta_k Re\left(\widehat{u}\left(\frac{\eta_k}{\tau}\right)\right), \tag{4.14}$$

where

$$\eta_k = \frac{N_e\ln(10)}{3} + \pi ik, \qquad \beta_k = (-1)^k\zeta_k, \tag{4.15}$$

with $i = \sqrt{-1}$ and $\zeta_0 = \frac{1}{2}$, $\zeta_k = 1$, $1 \leqslant k \leqslant N_e$, $\zeta_{2N_e} = \frac{1}{2^{N_e}}$,

$$\zeta_{2N_e-k} = \zeta_{2N_e-k+1} + 2^{-N_e}\binom{N_e}{k}, \quad 0 < k < N_e. \tag{4.16}$$

Convergence: The parameters in Eq. (4.14) were examined by the authors of [1] and its effect on the accuracy of the numerical solution was observed. According to their observations "for ξ significant are required, then let N_e be a positive-integer $\lceil 1.7\xi \rceil$. Set the system's precision at N_e. Calculate and the system's precision and η_k and β_k in (4.15) (4.16) for given N_e and system precision. Then for given function $\widehat{u}(s)$ and τ calculate $u_{ApSol}(\tau)$ in (4.14)".

4.2.4. Weeks method (WM)

In the literature, one of the simplest and most accurate numerical strategies for inverting the Laplace Transform (LT) is the Weeks method, provided the two parameters with optimal values are selected

for the Laguerre expansion. The Weeks approach has a notable benefit over the Talbot's method and trapezoidal rule: it provides a function expansion, specifically the Laguerre series expansion. In the proposed approach we select $s = \rho + i\eta$, $\eta \in \mathbb{R}$ to obtain

$$u_{\text{ApSol}}(\tau) = \frac{e^{\rho\tau}}{2\pi} \int_{-\infty}^{\infty} e^{i\tau\eta} \widehat{u}(\rho + i\eta) dy. \tag{4.17}$$

The function $\widehat{u}(\rho + i\eta)$ is expanded as

$$\widehat{u}(\rho + i\eta) = \sum_{\ell=-\infty}^{\infty} a_\ell \frac{(-\sigma + i\eta)^\ell}{(\sigma + i\eta)^{\ell+1}}, \ \sigma > 0, \ \eta \in \mathbb{R}. \tag{4.18}$$

Substituting (4.18) in (4.17), we have

$$u_{\text{ApSol}}(\tau) = \frac{e^{\rho\tau}}{2\pi} \sum_{\ell=-\infty}^{\infty} a_\ell \delta_\ell(\tau; \sigma),$$

where

$$\delta_\ell(\tau; \sigma) = \int_{-\infty}^{\infty} e^{i\tau\eta} \frac{(-\sigma + i\eta)^\ell}{(\sigma + i\eta)^{\ell+1}} d\eta.$$

One can calculate the Fourier integral, and for $\tau > 0$, we have

$$\delta_\ell(\tau; \sigma) = \begin{cases} 2\pi e^{-\sigma\tau} \mathcal{L}_\ell(2\sigma\tau), & \ell \geqslant 0, \\ 0, & \ell < 0, \end{cases}$$

where $\mathcal{L}_\ell(\tau)$ is Laguerre polynomial of degree ℓ, $\rho > \rho_0$, ρ_0 is the abscissa of convergence, and $\rho, \sigma \in \mathbb{R}^+$. The Laguerre polynomials $\mathcal{L}_\ell(\tau)$ are expressed as

$$\mathcal{L}_\ell(\tau) = \frac{e^\tau}{\ell!} \frac{d^\ell}{d\tau^\ell}(e^{-\tau}\tau^\ell),$$

where a_ℓ are the Taylor series expansion coefficients

$$\mathcal{M}(\zeta) = \frac{2\sigma}{1-\zeta} \widehat{u}\left(\rho + \frac{2\sigma}{1-\zeta} - \sigma\right) = \sum_{\ell=0}^{\infty} a_\ell \zeta^\ell, \ |\zeta| < R, \tag{4.19}$$

where R denotes radius of convergence of Maclaurin series (4.19), the unknowns a_ℓ are evaluated as

$$a_\ell = \frac{1}{2\pi i} \int_{|\zeta|=1} \frac{\mathcal{M}(\zeta)}{\zeta^{\ell+1}} d\zeta = \frac{1}{2\pi} \int_{-\pi}^{\pi} \mathcal{M}(e^{i\beta}) e^{-ik\beta} d\beta, \tag{4.20}$$

where (4.20) is the classic Cauchy integral formula, which is computed numerically as

$$\tilde{a}_\ell = \frac{e^{-i\ell k/2}}{2N_w} \sum_{j=-N_w}^{N_w-1} \mathcal{M}(e^{i\beta_{j+1}/2}) e^{-i\ell\beta_j}, \ \ell = 0, 1, 2, \ldots, N_w - 1,$$

where $\beta_j = jk$, $k = \frac{\pi}{N_w}$.

Error analysis: The authors of [59] examined the Weeks method's accuracy. Whilst they had been investigating the expansion

$$u(\tau) = \exp(\rho\tau) \sum_{\ell=0}^{\infty} a_\ell \exp(-\sigma\tau) \mathcal{L}_\ell(2\sigma\tau), \tag{4.21}$$

the following conclusions were made. Error was shown to be mainly caused by following three factors:

1st factor is the truncation error;
2nd the numerical evaluation of the unknown coefficients;
3rd the numerical inversion of LT, any inaccuracy during the evaluation of the unknown coefficients will increase with τ for $\rho > 0$, it explains how the error in (4.21) can be seen.

To study these errors, the actual expansion is

$$\tilde{u}(\tau) = \exp(\rho\tau) \sum_{\ell=0}^{N_w-1} \tilde{a}_\ell(1+\chi_\ell)\exp(-\sigma\tau)\mathcal{L}_\ell(2\sigma\tau), \tag{4.22}$$

χ_ℓ is the relative error in the floating-point representation of the coefficients, i.e., $fl(\tilde{a}_\ell) = \tilde{a}_\ell(1+\chi_\ell)$. From (4.22) and (4.21) we have

$$|u(\tau) - \tilde{u}(\tau)| \leqslant e^{(\rho\tau)}\Big(T_{err} + D_{err} + C_{err}\Big),$$

with assumption $\sum_{\ell=0}^{\infty}|a_\ell| < \infty$, where $T_{err} = \sum_{\ell=N_w}^{\infty}|a_\ell|$ is the truncation error bound,

$$D_{err} = \sum_{\ell=0}^{N_w-1}|a_\ell - \tilde{a}_\ell|$$

is the discretization error bound, $C_{err} = \chi\sum_{\ell=0}^{N_w-1}|\tilde{a}_\ell|$ is the conditioning error bound, and χ_ℓ denotes the roundoff unit of machine satisfying the condition $\max_{0\leqslant\ell\leqslant N_w-1}|\chi_\ell| \leqslant \chi$ with the fact that $|\exp(-\sigma\tau)\mathcal{L}_\ell(2\sigma\tau)| \leqslant 1$. We can neglect the D_{err} in comparison with T_{err} and C_{err} ([59]). Therefore, we refer to T_{err} and C_{err}. For T_{err} and C_{err} the upper bound were given by the author as [59]

$$T_{err} \leqslant \frac{\ell(\xi)}{\xi^{N_w}(\xi-1)},\ C_{err} \leqslant \chi\frac{\xi\ell(\xi)}{\xi-1},$$

which is true for $\xi \in (1, R)$. Hence, we have

$$error_{est} \leqslant \frac{\ell(\xi)}{\xi^{N_w}(\xi-1)} + \chi\frac{\xi\ell(\xi)}{\xi-1}.$$

5. Numerical results

Here, we provide the computational results of the suggested numerical methods for SPBVPs. The viability of the suggested numerical techniques is demonstrated using numerical examples. We conducted our experiments using MATLAB R2019a on a Windows 10 (64 bit) PC configured with an Intel(R) Core(TM) i5-3317U 1.70 GHz CPU and 12 GB of RAM. To measure the accuracy of the methods the maximum absolute error Er is used which is defined as $Er = \max_{1\leqslant i\leqslant N}|u(\tau_i) - u_{ApSol}(\tau_i)|$, where $u(\tau)$ is the analytical solution and $u_{ApSol}(\tau)$ is the approximate solution.

Problem 5.1. Here we consider a second order linear SPBVP of the form

$$-\epsilon\frac{d^2u(\tau)}{d\tau^2} + u(\tau) = \tau,\ \ 0 \leqslant \tau \leqslant 1,$$

with boundary conditions $u(0) = 1$ and $u(1) = 1 + e^{\frac{-1}{\sqrt{\epsilon}}}$, with exact solution

$$u(\tau) = \tau + e^{\frac{-\tau}{\sqrt{\epsilon}}}.$$

The simulation results of the four proposed numerical methods are presented in Table 3. The exact and approximate solutions are plotted in Figure 6 using the ITM. The absolute errors obtained using the LRBFM, the EM, the ITM, and the WM are presented in Figures 7-10. It is easily verified from Table 3 that our techniques give accurate and stable results for various values of ϵ. Table 3 shows that the numerical solutions obtained via the suggested numerical methods are in nice agreement with the exact solution as compared to the numerical solution of [7]. We conclude that the results of the proposed numerical schemes are better for such type of SPBVPs.

Table 3: The simulation results of the four proposed methods for Problem 5.1.

ϵ	2^{-4}	2^{-5}	2^{-6}	2^{-7}	2^{-8}
LRBFM					
$(N_r, ns) = (135, 5)$	3.2868×10^{-5}	3.2261×10^{-5}	3.1033×10^{-5}	2.9610×10^{-5}	2.7736×10^{-5}
$(N_r, ns) = (145, 5)$	2.3365×10^{-5}	2.2610×10^{-5}	2.1585×10^{-5}	2.0216×10^{-5}	1.8433×10^{-5}
$(N_r, ns) = (155, 5)$	1.2488×10^{-5}	1.2296×10^{-5}	1.2254×10^{-5}	1.2254×10^{-5}	1.3408×10^{-5}
$(N_r, ns) = (165, 5)$	2.1855×10^{-5}	1.2477×10^{-5}	1.2309×10^{-5}	1.2305×10^{-5}	1.2305×10^{-5}
EM					
$N_e = 15$	3.0143×10^{-10}	3.3044×10^{-10}	3.4648×10^{-10}	3.3950×10^{-10}	2.9124×10^{-10}
$N_e = 16$	5.2998×10^{-11}	5.2930×10^{-11}	5.4630×10^{-11}	4.9735×10^{-11}	6.7736×10^{-11}
$N_e = 17$	1.8879×10^{-11}	1.4098×10^{-11}	9.1822×10^{-12}	1.8578×10^{-11}	1.2262×10^{-11}
$N_e = 18$	1.9334×10^{-11}	2.0401×10^{-12}	1.6474×10^{-11}	1.1262×10^{-11}	3.3382×10^{-12}
ITM					
$N_t = 20$	4.1999×10^{-10}	4.1857×10^{-10}	4.1869×10^{-10}	4.1904×10^{-10}	4.1918×10^{-10}
$N_t = 22$	4.1918×10^{-10}	3.0826×10^{-11}	3.0791×10^{-11}	3.0768×10^{-11}	3.0758×10^{-11}
$N_t = 24$	2.2347×10^{-12}	2.2400×10^{-12}	2.2393×10^{-12}	2.2398×10^{-12}	2.2407×10^{-12}
$N_t = 28$	4.0191×10^{-14}	3.6861×10^{-14}	2.9978×10^{-14}	2.9089×10^{-14}	2.7535×10^{-14}
WM					
$N_w = 20$	4.2188×10^{-15}	3.9524×10^{-14}	7.9137×10^{-13}	3.9668×10^{-11}	1.9445×10^{-09}
$N_w = 25$	6.6613×10^{-16}	8.8818×10^{-16}	4.4409×10^{-16}	9.1038×10^{-15}	1.9276×10^{-12}
$N_w = 30$	2.2204×10^{-16}	0	1.1102×10^{-15}	1.7764×10^{-15}	2.3315×10^{-14}
$N_w = 35$	0	2.2204×10^{-16}	0	0	1.5543×10^{-15}
[7]	6.8842×10^{-8}	1.1283×10^{-7}	4.4143×10^{-7}	5.0019×10^{-7}	5.4573×10^{-7}

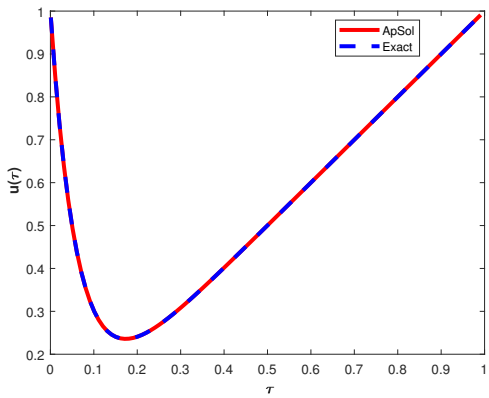

Figure 6: The exact (Exact) and numerical (ApSol) solutions of Problem 5.1 using ITM with $N_t = 28$ and $\epsilon = 2^{-8}$.

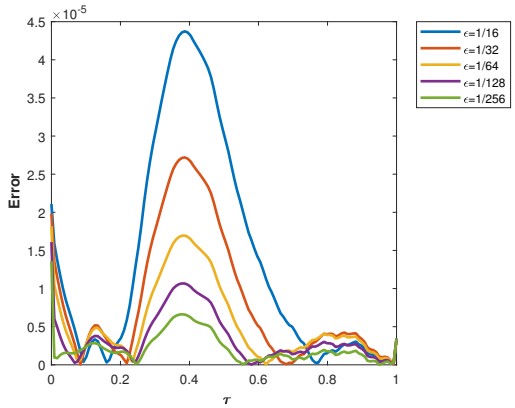

Figure 7: The plot of Er via the LRBFM for Problem 5.1 with $N_r = 120$ and $n = 9$.

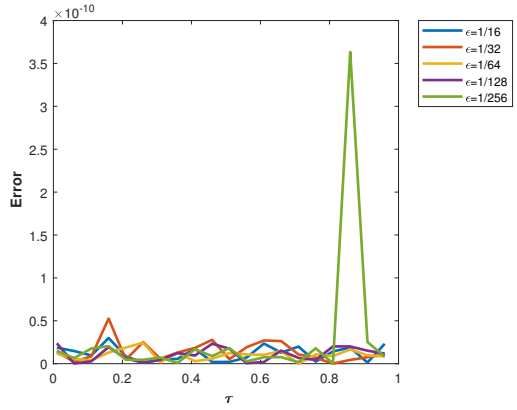

Figure 8: The plot of Er via the EM for Problem 5.1 with $N_e = 18$.

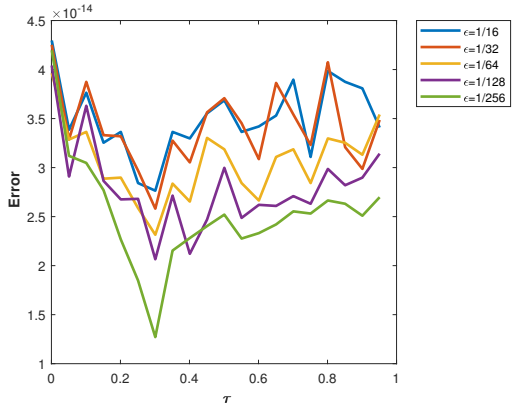

Figure 9: The plot of Er via the ITM for Problem 5.1 with $N_t = 28$.

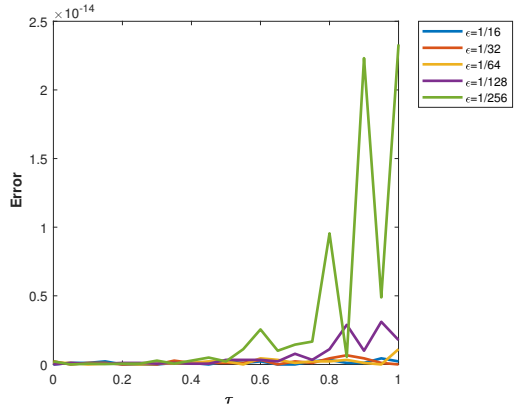

Figure 10: The plot of Er via the WM for Problem 5.1 with $N_w = 30$.

[h!]

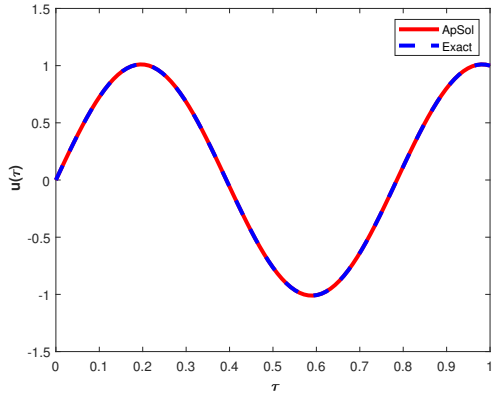

Figure 11: The exact (Exact) and numerical (ApSol) solutions of Problem 5.2 using LRBFM with $N_\tau = 99$, $n = 5$, and $\epsilon = 2^{-6}$.

Problem 5.2. Here we consider a second order linear SPBVP of the form

$$\frac{d^2u(\tau)}{d\tau^2} + \epsilon u(\tau) = 0, \quad 0 \leqslant \tau \leqslant 1,$$

with boundary conditions $u(0) = 1$ and $u(1) = 1$, with exact solution $u(\tau) = \frac{\sin\frac{\tau}{\sqrt{\epsilon}}}{\sin\frac{1}{\sqrt{\epsilon}}}$. The simulation results of the four proposed methods are depicted in Table 4. In Figure 11 we present a comparison between the exact and numerical solution obtained using the LRBFM. The graphical illustration of absolute errors obtained using the LRBFM, the EM, the ITM, and the WM for various values of ϵ are presented in Figures 12-15. Table 4 presents a comparison of absolute errors of the four proposed numerical schemes for different values of the parameter ϵ with the absolute error of GRBFM [7]. We can see the EM, the ITM, and the WM have approximated the solution of SPBVPs efficiently and accurately as compared to GRBFM [7].

Problem 5.3. Here we consider a second order linear SPBVP of the form

$$-\epsilon\frac{d^2u(\tau)}{d\tau^2} + \frac{du(\tau)}{d\tau} = \epsilon\pi^2\sin(\pi\tau) + \pi\cos(\pi\tau), \quad 0 \leqslant \tau \leqslant 1,$$

with boundary conditions $u(0) = 0$ and $u(1) = 0$, with exact solution $u(\tau) = \sin(\pi\tau)$. The simulation results of the four proposed numerical methods are presented in Table 5. The exact solution of the problem and the numerical solution obtained via the LRBFM are compared in Figure 16. A comparison

Table 4: The simulation results of the four proposed methods for Problem 5.2.

ϵ	2^{-2}	2^{-3}	2^{-4}	2^{-5}	2^{-6}
LRBFM					
$(N_r, ns) = (143, 3)$	4.8386×10^{-5}	5.2258×10^{-4}	1.3577×10^{-4}	1.0225×10^{-3}	8.8189×10^{-4}
$(N_r, ns) = (145, 3)$	7.5139×10^{-5}	7.6138×10^{-4}	3.2947×10^{-5}	3.3412×10^{-4}	5.9154×10^{-4}
$(N_r, ns) = (147, 3)$	8.3786×10^{-5}	1.1981×10^{-3}	1.1970×10^{-4}	7.9011×10^{-5}	4.6007×10^{-4}
EM					
$N_e = 14$	4.7103×10^{-11}	2.0456×10^{-09}	1.9342×10^{-10}	3.8004×10^{-10}	8.8895×10^{-10}
$N_e = 16$	7.6725×10^{-12}	1.1778×10^{-10}	2.2761×10^{-11}	4.5691×10^{-11}	7.2315×10^{-11}
$N_e = 18$	1.8157×10^{-12}	6.9169×10^{-12}	4.4202×10^{-12}	4.2526×10^{-12}	1.5797×10^{-12}
ITM					
$N_t = 56$	1.1651×10^{-12}	4.6700×10^{-12}	2.5655×10^{-12}	4.4092×10^{-12}	2.0795×10^{-11}
$N_t = 58$	2.0091×10^{-12}	8.1861×10^{-12}	4.5642×10^{-12}	7.2183×10^{-12}	4.2448×10^{-12}
$N_t = 60$	2.3400×10^{-13}	5.4272×10^{-13}	5.1985×10^{-13}	7.6566×10^{-13}	1.3834×10^{-12}
WM					
$N_w = 25$	3.3307×10^{-16}	2.8866×10^{-16}	6.7280×10^{-14}	5.1725×10^{-12}	6.4269×10^{-09}
$N_w = 30$	4.4409×10^{-16}	0	4.3299×10^{-15}	1.6087×10^{-13}	3.4131×10^{-11}
$N_w = 35$	0	2.2204×10^{-16}	6.6613×10^{-16}	2.6645×10^{-15}	1.1102×10^{-14}
[7]	5.9287×10^{-7}	3.7321×10^{-6}	2.3293×10^{-6}	5.7657×10^{-5}	9.5596×10^{-5}

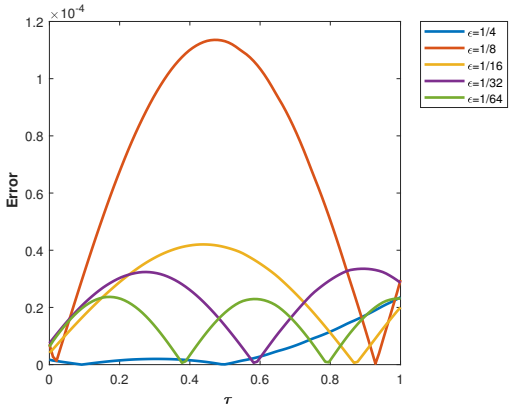

Figure 12: The plot of Er via the LRBFM for Problem 5.2 with $N_r = 99$ and $n = 5$.

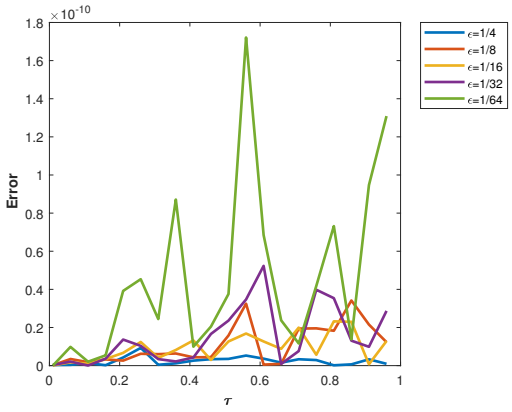

Figure 13: The plot of Er via the EM for Problem 5.2 with $N_e = 22$.

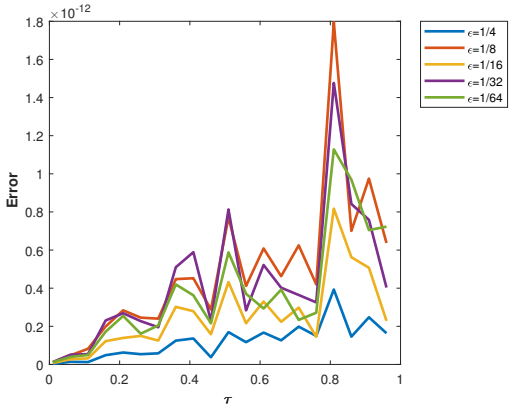

Figure 14: The plot of Er via the ITM for Problem 5.2 with $N_t = 60$.

[h!]

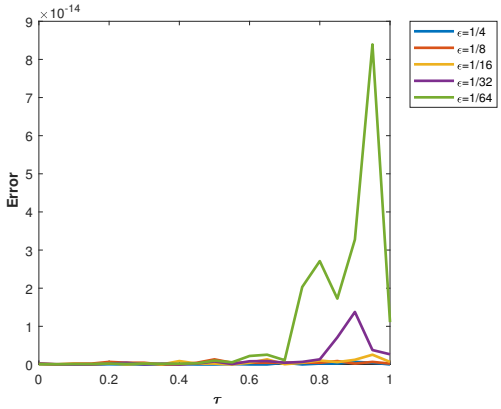

Figure 15: The plot of Er via the WM for Problem 5.2 with $N_w = 35$.

of absolute errors obtained using the LRBFM, the EM, the ITM, and the WM for various values of ϵ is presented in Figures 17-20. We see that for all the suggested numerical methods the accuracy increases with increasing the number of nodes. It has been noticed that all the four methods gives accurate and stable results. The comparison of absolute errors of the suggested numerical schemes with the absolute error of finite difference scheme [21] is shown in Table 5. The findings demonstrate that the proposed numerical schemes yield accurate outcomes.

Table 5: The simulation results of the four proposed methods for Problem 5.3.

ϵ	10^{-1}	10^{-2}	10^{-3}	10^{-4}	10^{-5}
LRBFM					
$(N_r, ns) = (90, 5)$	6.5975×10^{-6}	2.2620×10^{-5}	2.3219×10^{-5}	2.1518×10^{-5}	2.1518×10^{-5}
$(N_r, ns) = (100, 5)$	4.9814×10^{-5}	2.1468×10^{-6}	1.7536×10^{-6}	1.679×10^{-6}	1.6002×10^{-6}
$(N_r, ns) = (110, 5)$	3.5865×10^{-5}	4.7597×10^{-6}	5.6790×10^{-6}	6.5696×10^{-6}	6.2798×10^{-6}
$(N_r, ns) = (120, 5)$	1.8811×10^{-6}	1.4976×10^{-6}	1.6061×10^{-6}	1.6525×10^{-6}	1.5774×10^{-6}
EM					
$N_e = 15$	7.7888×10^{-11}	7.9918×10^{-11}	8.0356×10^{-11}	8.0217×10^{-11}	7.9536×10^{-11}
$N_e = 16$	2.3088×10^{-11}	2.2306×10^{-11}	2.1312×10^{-11}	2.1526×10^{-11}	2.0640×10^{-11}
$N_e = 17$	4.2501×10^{-12}	4.6905×10^{-12}	4.2645×10^{-12}	1.0137×10^{-12}	3.5222×10^{-12}
$N_e = 18$	6.0857×10^{-13}	4.5890×10^{-12}	4.2906×10^{-12}	1.4062×10^{-12}	4.5998×10^{-12}
ITM					
$N_t = 38$	1.9564×10^{-12}	1.9614×10^{-12}	1.9562×10^{-12}	1.9591×10^{-12}	1.9556×10^{-12}
$N_t = 40$	1.5570×10^{-12}	1.5454×10^{-12}	1.5524×10^{-12}	1.5455×10^{-12}	1.5538×10^{-12}
$N_t = 42$	6.2705×10^{-13}	6.1079×10^{-13}	6.1190×10^{-13}	6.0378×10^{-13}	6.0970×10^{-13}
$N_t = 44$	4.0050×10^{-13}	4.1531×10^{-13}	4.2403×10^{-13}	4.0517×10^{-13}	4.2104×10^{-13}
WM					
$N_w = 20$	4.5765×10^{-14}	1.0636×10^{-13}	1.3906×10^{-13}	1.3578×10^{-13}	1.9801×10^{-14}
$N_w = 25$	9.3805×10^{-15}	1.8711×10^{-15}	2.6449×10^{-15}	4.3463×10^{-16}	2.0640×10^{-15}
$N_w = 30$	5.8976×10^{-16}	8.5283×10^{-16}	2.9222×10^{-16}	5.7803×10^{-16}	1.0008×10^{-16}
$N_w = 35$	2.7933×10^{-16}	3.8858×10^{-16}	6.2709×10^{-16}	8.4146×10^{-16}	4.2057×10^{-17}
[21]	8.72×10^{-7}	3.41×10^{-7}	1.42×10^{-6}	1.68×10^{-6}	1.72×10^{-6}

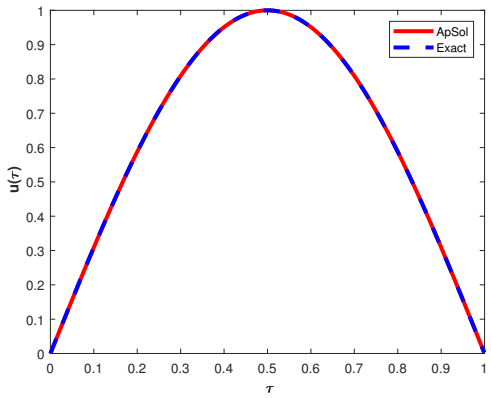

Figure 16: The exact (Exact) and numerical (ApSol) solutions of Problem 5.3 using EM with $N_e = 18$ and $\epsilon = 10^{-5}$.

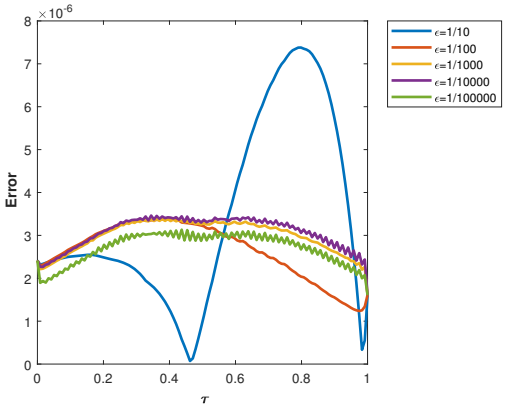

Figure 17: The plot of Er via the LRBFM for Problem 5.3 with $N_r = 120$ and $n = 5$.

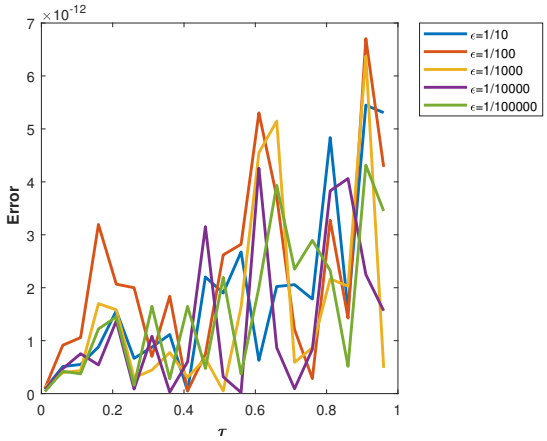

Figure 18: The plot of Er via the EM for Problem 5.3 with $N_e = 18$.

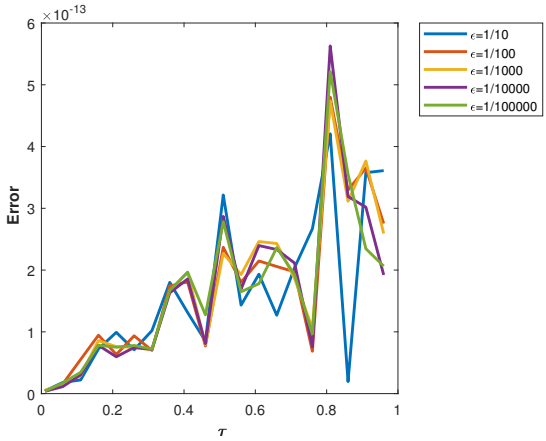

Figure 19: The plot of Er via the ITM for Problem 5.3 with $N_t = 60$.

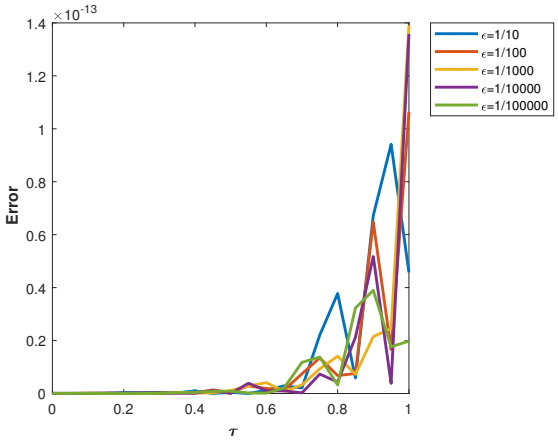

Figure 20: The plot of Er via the WM for Problem 5.3 with $N_w = 20$.

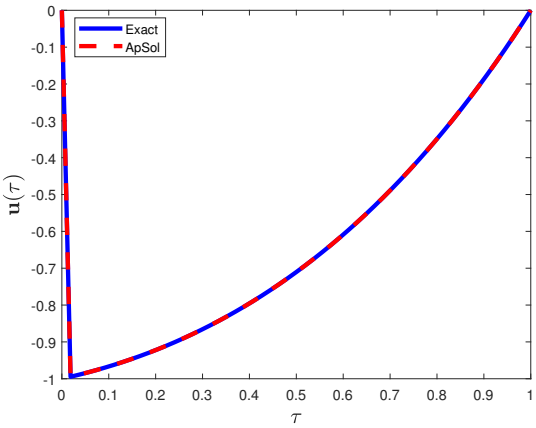

Figure 21: The exact and approximate solutions of Problem 5.4 using LRBFM with $N_r = 55$ and $n = 5$ and $\epsilon = 5^{-6}$.

Problem 5.4. Here we consider a second order linear SPBVP with left-end boundary layer

$$-\epsilon^2 \frac{d^2u(\tau)}{d\tau^2} + u(\tau) = (-\epsilon^2 + 1)e^{\tau} - \tau(e + e^{-1/\epsilon}) - 2(1-\tau), \quad 0 \leqslant \tau \leqslant 1,$$

with boundary condition $u(0) = 0$ and $u(1) = 0$, with exact solution $u(\tau) = e^{-\tau/\epsilon} + e^{\tau} - \tau(e + e^{-1/\epsilon}) - 2(1-\tau)$. The simulation results of the four proposed methods are shown in Table 6. Figure 21 shows the exact and numerical solution computed using the LRBFM. A comparison of absolute errors obtained using the LRBFM, the EM, the ITM, and the WM for various values of ϵ is presented in Figures 22-25. One can see that the error between the exact solution and approximate solution decays by increasing the number of nodes for each method. Also for the LRBFM, the EM, and ITM the accuracy is not effected much by varying the value of the parameter ϵ. However, for the WM the accuracy decreases as we decrease the value of the parameter ϵ. Table 6 shows that our numerical methods are considerably accurate in comparison with the method in [44].

Table 6: The simulation results of the four proposed methods for Problem 5.4.

ϵ	5^{-2}	5^{-3}	5^{-4}	5^{-5}	5^{-6}
LRBFM					
$(N_r, ns) = (145, 7)$	1.4916×10^{-5}	2.1773×10^{-3}	2.6502×10^{-2}	1.6506×10^{-3}	6.6124×10^{-5}
$(N_r, ns) = (150, 7)$	7.7785×10^{-6}	1.9319×10^{-3}	2.7118×10^{-2}	1.7675×10^{-3}	7.0814×10^{-5}
$(N_r, ns) = (155, 7)$	8.6312×10^{-6}	1.7160×10^{-3}	2.7636×10^{-2}	1.8877×10^{-3}	7.5640×10^{-5}
EM					
$N_e = 14$	7.2078×10^{-9}	7.1432×10^{-09}	7.1413×10^{-9}	7.1412×10^{-9}	7.1412×10^{-9}
$N_e = 16$	3.3499×10^{-10}	3.2540×10^{-10}	3.2515×10^{-10}	3.2997×10^{-11}	3.2500×10^{-10}
$N_e = 18$	3.7393×10^{-11}	2.1182×10^{-11}	1.4187×10^{-11}	1.4737×10^{-11}	3.3979×10^{-11}
ITM					
$N_t = 36$	1.4741×10^{-12}	1.5226×10^{-12}	1.5520×10^{-12}	1.5483×10^{-12}	1.5480×10^{-12}
$N_t = 38$	2.7519×10^{-13}	2.9375×10^{-13}	2.9339×10^{-13}	2.9948×10^{-13}	2.9406×10^{-13}
$N_t = 40$	9.2418×10^{-14}	8.2851×10^{-14}	7.7848×10^{-14}	7.8564×10^{-14}	9.3106×10^{-14}
WM					
$N_w = 50$	3.8964×10^{-16}	2.7529×10^{-5}	2.0384×10^{-3}	4.0179×10^{-4}	7.9966×10^{-5}
$N_w = 55$	3.1130×10^{-15}	2.9396×10^{-5}	3.6532×10^{-3}	8.4867×10^{-4}	1.6865×10^{-4}
$N_w = 60$	2.8896×10^{-15}	3.1968×10^{-5}	2.0331×10^{-3}	1.0858×10^{-3}	2.1546×10^{-4}
[44]	2.8906×10^{-5}	5.8909×10^{-6}	1.2027×10^{-7}	1.2907×10^{-7}	3.8111×10^{-7}

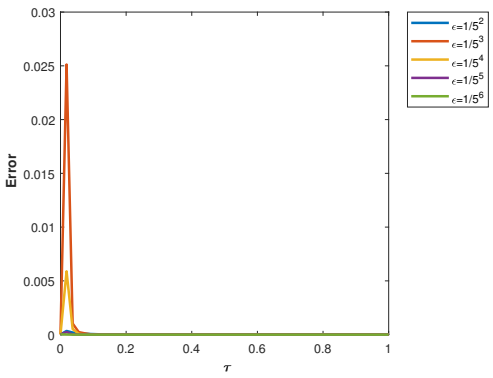

Figure 22: The plot of Er via the LRBFM for Problem 5.4 with $N_r = 55$ and $n = 7$.

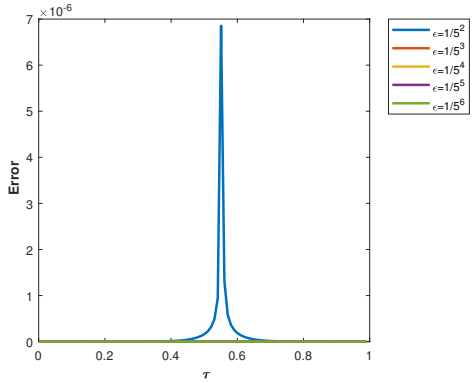

Figure 23: The plot of Er via the EM for Problem 5.4 with $N_e = 18$.

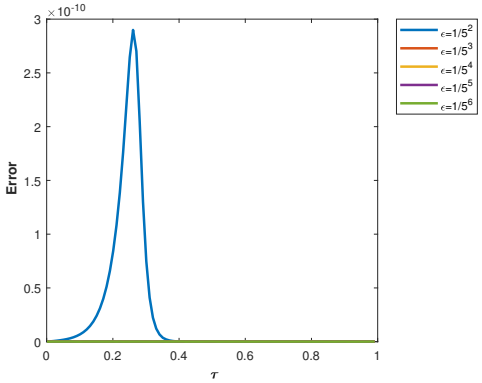

Figure 24: The plot of Er via the ITM for Problem 5.4 with $N_t = 40$.

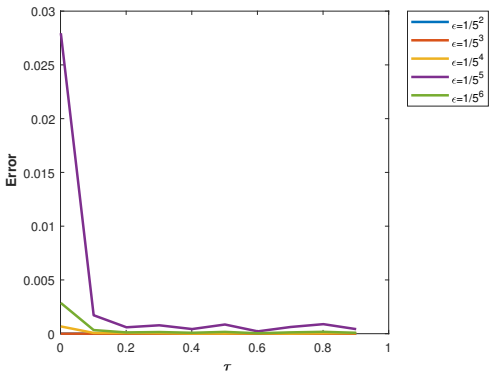

Figure 25: The plot of Er via the WM for Problem 5.4 with $N_w = 200$.

6. Conclusion

A comparison of LRBFM, Talbot's, Euler's, and Weeks method for the numerical solution of SPBVPs is performed in this paper. Four linear SPBVPs with different values of the perturbed perimeter ϵ were solved using the proposed numerical methods. The results obtained using these methods were compared with each other and with other methods available in literature. The numerical evidence shows superiority of the suggested numerical methods in terms of fast convergence and better accuracy. However, in these four suggested numerical methods the Weeks method gives more accurate and stable results for all problems. We also noticed that the proposed numerical methods are easy to implement, require less computational time, and provide more quantitatively reliable results. The proposed numerical methods can safely and quickly be used for the solution of a wide range of similar problems

Acknowledgment

The first author, S. Aljawi, expresses her gratitude to Princess Nourah bint Abdulrahman University Researchers Supporting Project (no. PNURSP2024R514), Princess Nourah bint Abdulrahman University, Riyadh, Saudi Arabia. The authors D. Santina and N. Mlaiki would like to thank Prince Sultan University for paying the article publication fees and for the support through the TAS research lab.

References

[1] J. Abate, W. Whitt, *A unified framework for numerically inverting Laplace transforms*, INFORMS J. Comput., **18** (2006), 408–421. 1, 4.2.3
[2] T. Abdeljawad, A. Younus, M. A. Alqudah, U. Atta, *On fuzzy conformable double Laplace transform with applications to partial differential equations*, Comput. Model. Eng. Sci., **134** (2023), 2163–2191. 1
[3] R. P. Agarwal, M. Meehan, D. O'regan. *Fixed point theory and applications*, Cambridge University Press, Cambridge, (2001). 2.3
[4] S. Ahmed, S. Jahan, K. J. Ansari, K. Shah, T. Abdeljawad, *Wavelets collocation method for singularly perturbed differential difference equations arising in control system*, Results Appl. Math., **21** (2024), 13 pages. 1
[5] M. Ahsan, M. Bohner, A. Ullah, A. A. Khan, S. Ahmad, *A Haar wavelet multi-resolution collocation method for singularly perturbed differential equations with integral boundary conditions*, Math. Comput. Simul., **204** (2023), 166–180. 1
[6] A. Ali, J. F. Gómez-Aguilar, *A transform based local RBF method for 2D linear PDE with Caputo-Fabrizio derivative*, C. R. Math. Acad. Sci. Paris, **358** (2020), 831–842. 1
[7] I. Ali, S. Haq, R. Ullah, S. U. Arifeen, *Approximate Solution of Second Order Singular Perturbed and Obstacle Boundary Value Problems Using Meshless Method Based on Radial Basis Functions*, J. Nonlinear Math. Phys., **30** (2023), 215–234. 1, 5.1, 3, 5.2, 4
[8] Z. Avazzadeh, O. Nikan, J. Tenreiro Machado, M. N. Rasoulizadeh, *Numerical analysis of time-fractional Sobolev equation for fluid-driven processes in impermeable rocks*, Adv. Contin. Discrete Models, **202** (2022), 14 pages. 1
[9] I. A. Bhat, L. N. Mishra, V. N. Mishra, C. Tunç, O. Tunç, *Precision and efficiency of an interpolation approach to weakly singular integral equations*, Int. J. Numer. Methods Heat Fluid Flow, **34** (2024), 1479–1499. 1
[10] H. G. Debela, S. B. Kejela, A. D. Negassa. *Exponentially Fitted Numerical Method for Singularly Perturbed Differential-Difference Equations*, Int. J. Differ. Equ., **2020** (2020), 13 pages. 1
[11] H. G. Debela, G. F. Duressa, *Accelerated fitted operator finite difference method for singularly perturbed delay differential equations with non-local boundary condition*, J. Egypt. Math. Soc., **28** (2020), 16 pages. 1
[12] B. Dingfelder, J. A. C. Weideman, *An improved Talbot method for numerical Laplace transform inversion*, Numer. Algorithms, **68** (2015), 167–183. 1, 4.2.1, 4.1, 4.2.2
[13] I. P. Gavrilyuk, V. L. Makarov, *Exponentially convergent algorithms for the operator exponential with applications to inhomogeneous problems in Banach spaces*, SIAM J. Numer. Anal., **43** (2005), 2144–2171. 4.2.1
[14] F. Z. Geng, S. P. Qian, S. Li, *A numerical method for singularly perturbed turning point problems with an interior layer*, J. Comput. Appl. Math., **255** (2014), 97–105. 1
[15] M.B. Ghaemi, M. E. Gordji, B. Alizadeh, C. Park, *Hyers-Ulam stability of exact second-order linear differential equations*, Adv. Differ. Equ., **2012** (2012), 7 pages.
[16] V. Y. Glizer, *Asymptotic analysis and solution of a finite-horizon H_∞ control problem for singularly-perturbed linear systems with small state delay*, J. Optim. Theory. Appl., **117** (2003), 295–325. 1
[17] D. J. Halsted, D. E. Brown, *Zakian's technique for inverting Laplace transforms*, Chem. Eng. J., **3** (1972), 312–313. 1
[18] P. Hammachukiattikul, E. Sekar, A. Tamilselvan, R. Vadivel, N. Gunasekaran, P. Agarwal, *Comparative study on numerical methods for singularly perturbed advanced-delay differential equations*, J. Math., **2021** (2021), 15 pages. 1

[19] H. Hassanzadeh, M. Pooladi-Darvish, *Comparison of different numerical Laplace inversion methods for engineering applications*, Appl. Math. Comput., **189** (2007), 1966–1981. 1

[20] G. Honig, U. Hirdes. *A method for the numerical inversion of Laplace transforms*, J. Comput. Appl. Math., **10** (1984), 113–132. 1

[21] F. O. Ilicasu, D. H. Schultz. *High-order finite-difference techniques for linear singular perturbation boundary value problems*, Comput. Math. Appl., **47** (2004), 391–417. 5.3, 5

[22] S. Jelbart, N. Pages, V. Kirk, J. Sneyd, M. Wechselberger, *Process-oriented geometric singular perturbation theory and calcium dynamics*, SIAM J. Appl. Dyna. Syst., **21** (2022), 982–1029. 1

[23] M. K. Kadalbajoo, P. Arora, V. Gupta, *Collocation method using artificial viscosity for solving stiff singularly perturbed turning point problem having twin boundary layers*, Comput. Math. Appl., **61** (2011), 1595–1607. 1

[24] Kamran, M. Irfan, F. M. Alotaibi, S. Haque, N. Mlaiki, K. Shah, *RBF-based local meshless method for fractional diffusion equations*, Fractal Fract., **7** (2023), 21 pages. 1

[25] Kamran, S. U. Khan, S. Haque, N. Mlaiki, *On the Approximation of Fractional-Order Differential Equations Using Laplace Transform and Weeks Method*, Symmetry, **15** (2023), 16 pages. 1

[26] M. Kumar, P. Singh, H. K. Mishra, *An initial-value technique for singularly perturbed boundary value problems via cubic spline*, Int. J. Comput. Methods Eng. Sci. Mech., **8** (2007), 419–427 1

[27] C. K. Lee, X. Liu, S. C. Fan. *Local multiquadric approximation for solving boundary value problems*, Comput. Mech., **30** (2003), 396–409. 4.1

[28] E. Liz, C. Lois-Prados, *A note on the Lasota discrete model for blood cell production*, Discrete Contin. Dyn. Syst. Ser. B, **25** (2020), 701–713. 1

[29] A. Luongo, S. Casciati, D. Zulli, *Perturbation method for the dynamic analysis of a bistable oscillator under slow harmonic excitation*, Smart Struct. Syst., **18** (2016), 183–196. 1

[30] M. Marušić, *On ε-uniform convergence of exponentially fitted methods*, Math. Commun., **19** (2014), 545–559. 1

[31] S. Natesan, J. Jayakumar, J. Vigo-Aguiar, *Parameter uniform numerical method for singularly perturbed turning point problems exhibiting boundary layers*, J. Comput. Appl. Math., **158** (2003), 121–134. 1

[32] A. H. Nayfeh, *Perturbation Methods*, John Wiley & Sons, New York-London-Sydney, (1973). 1

[33] N. N. Nefedov, L. Recke, K. R. Schneider, *Existence and asymptotic stability of periodic solutions with an interior layer of reaction advection diffusion equations*, J. Math. Anal. Appl., **405** (2013), 90–103. 1

[34] O. Nikan, Z. Avazzadeh, J. A. T. Machado, *A local stabilized approach for approximating the modified time-fractional diffusion problem arising in heat and mass transfer*, J. Adv. Res., **32** (2021), 45–60. 1

[35] A. Noorizadegan, D. L. Young, C.-S. Chen, *A novel local radial basis function collocation method for multi-dimensional piezoelectric problems*, J. Intell. Mater. Syst. Struct., **33** (2022), 1574–1587. 1

[36] C. E. Pearson, *On a differential equation of boundary layer type*, J. Math. Phys., **47** (1968), 134–154. 1

[37] K. Phaneendra, Y. N. Reddy, G. B. S. L. Soujanya, *Non-iterative numerical integration method for singular perturbation problems exhibiting internal and twin boundary layers*, Int. J. Appl. Math. Comput., **3** (2011), 9–20. 1

[38] J. Quinn, *A numerical method for a nonlinear singularly perturbed interior layer problem using an approximate layer location*, J. Comput. Appl. Math., **290** (2015), 500–515. 1

[39] P. Rai, K. K. Sharma. *Numerical study of singularly perturbed differential difference equation arising in the modeling of neuronal variability*, Comput. Math. Appl., **63** (2012), 118–132. 1

[40] H. Ramos, J. Vigo-Aguiar, S. Natesan, R. García-Rubio, M. A. Queiruga, *Numerical solution of nonlinear singularly perturbed problems on nonuniform meshes by using a non-standard algorithm*, J. Math. Chem., **48** (2010), 38–54. 1

[41] M. Safinejad, M. M. Moghaddam, *A local meshless RBF method for solving fractional integro-differential equations with optimal shape parameters*, Ital. J. Pure Appl. Math., **41** (2019), 382–398. 1

[42] B. Šarler, R. Vertnik, *Meshfree explicit local radial basis function collocation method for diffusion problems*, Comput. Math. Appl., **51** (2006), 1269–1282. 1

[43] R. Schaback. *Error estimates and condition numbers for radial basis function interpolation*, Adv. Comput. Math., **3** (1995), 251–264. 4.1.1

[44] F. A. Shah, R. Abass, J. Iqbal, *Numerical solution of singularly perturbed problems using Haar wavelet collocation method*, Cogent Math., **3** (2016), 13 pages. 5.4, 6

[45] F. A. Shah, Kamran, W. Boulila, A. Koubaa, N. Mlaiki, *Numerical Solution of Advection-Diffusion Equation of Fractional Order Using Chebyshev Collocation Method*, Fractal Fract., **7** (2023), 20 pages. 1

[46] F. A. Shah, Kamran, D. Santina, N. Mlaiki, S. Aljawi, *Application of a hybrid pseudospectral method to a new two-dimensional multi-term mixed sub-diffusion and wave-diffusion equation of fractional order*, Netw. Heterog. Media, **19** (2024), 44–85. 1

[47] F. A. Shah, Kamran, K. Shah, T. Abdeljawad, *Numerical modelling of advection diffusion equation using Chebyshev spectral collocation method and Laplace transform*, Results Appl. Math., **21** (2024), 16 pages. 1

[48] D. Sheen, I. H. Sloan, V. Thomée, *A parallel method for time discretization of parabolic equations based on Laplace transformation and quadrature*, IMA J. Numer. Anal., **23** (2003), 269–299. 4.2.1

[49] J. L. Schiff, *The Laplace transform: theory and applications*, Springer-Verlag, New York, (1999) 1

[50] Siraj-ul-Islam, R. Vertnik, B. Šarler, *Local radial basis function collocation method along with explicit time stepping for hyperbolic partial differential equations*, Appl. Numer. Math., **67** (2013), 136–151. 1

[51] H. Stehfest, *Algorithm 368: Numerical inversion of Laplace transforms [D5]*, Commun. ACM., **13** (1970), 47–49. 1

[52] A. Talbot, *The accurate numerical inversion of Laplace transforms*, J. Inst. Math. Appl., **23** (1979), 97–120. 1, 4.2.1
[53] L. N. Trefethen, D. Bau III,, *Numerical linear algebra*, Society for Industrial and Applied Mathematics (SIAM), Philadelphia, PA, (1997). 4.1.1
[54] O. Tunç, C. Tunç, *Ulam stabilities of nonlinear iterative integro-differential equations*, Rev. R. Acad. Cienc. Exactas Fís. Nat. Ser. A Mat. RACSAM, **117** (2023), 18 pages. 2.2
[55] O. Tunç, C. Tunç, *On Ulam stabilities of iterative Fredholm and Volterra integral equations with multiple time-varying delays*, Rev. R. Acad. Cienc. Exactas Fís. Nat. Ser. A Mat. RACSAM, **118** (2024), 20 pages. 1
[56] J. Vigo-Aguiar, S. Natesan, *An efficient numerical method for singular perturbation problems*, J. Comput. Appl. Math., **192** (2006), 132–141. 1
[57] A.-M. Wazwaz, *Linear and nonlinear integral equations*, Higher Education Press, Beijing; Springer, Heidelberg, (2011). 2.1
[58] S. Wei, W. Chen, Y. Zhang, H. Wei, R. M. Garrard, *A local radial basis function collocation method to solve the variable-order time fractional diffusion equation in a two-dimensional irregular domain*, Numer. Methods Partial Differ. Equ., **34** (2018), 1209–1223. 1
[59] J. A. C. Weideman, *Algorithms for parameter selection in the Weeks method for inverting the Laplace transform*, SIAM J. Sci. Comput., **21** (1999), 111–128. 1, 4.2.4, 4.2.4
[60] G. Yao, Z. Yu, *A localized meshless approach for modeling spatial-temporal calcium dynamics in ventricular myocytes*, Int. J. Numer. Methods Biomed. Eng., **28** (2012), 187–204. 1
[61] A. Younus, M. Asif, U. Atta, T. Bashir, T. Abdeljawad, *Applications of fuzzy conformable Laplace transforms for solving fuzzy conformable differential equations*, Soft Comput., **27** (2023), 8583–8597. 1